Radboud Repository

Radboud University Nijmegen

PDF hosted at the Radboud Repository of the Radboud University Nijmegen

The following full text is a preprint version which may differ from the publisher's version.

For additional information about this publication click this link.
http://hdl.handle.net/2066/75216

Please be advised that this information was generated on 2018-07-08 and may be subject to change.

arXiv:0910.4745v1 [astro-ph.HE] 25 Oct 2009

Improved flux limits for neutrinos with energies above 10^{22} eV from observations with the Westerbork Synthesis Radio Telescope

O. Scholten,[1] S. Buitink,[2,3] J. Bacelar,[4] R. Braun,[5] A.G. de Bruyn,[6,7]
H. Falcke,[2] K. Singh,[1] B. Stappers,[8] R.G. Strom,[7,9] and R. al Yahyaoui[1]
[1]*Kernfysisch Versneller Instituut, University of Groningen, 9747 AA, Groningen, The Netherlands*
[2] *Department of Astrophysics, IMAPP, Radboud University, 6500 GL Nijmegen, The Netherlands*
[3]*Lawrence Berkeley National Laboratory, Berkeley, California 94720, USA*
[4]*ASML Netherlands BV, P.O.Box 324, 5500 AH Veldhoven, The Netherlands*
[5]*CSIRO-ATNF, P.O.Box 76, Epping NSW 1710, Australia*
[6]*Kapteyn Institute, University of Groningen, 9747 AA, Groningen, The Netherlands*
[7]*ASTRON, 7990 AA Dwingeloo, The Netherlands*
[8]*Jodrell Bank Centre for Astrophysics, School of Physics and Astronomy,*
The University of Manchester, Manchester M13 9PL, UK
[9]*Astronomical Institute 'A. Pannekoek', University of Amsterdam, 1098 SJ, The Netherlands*

Particle cascades initiated by ultra-high energy (UHE) neutrinos in the lunar regolith will emit an electromagnetic pulse with a time duration of the order of nano seconds through a process known as the Askaryan effect. It has been shown that in an observing window around 150 MHz there is a maximum chance for detecting this radiation with radio telescopes commonly used in astronomy. In 50 hours of observation time with the Westerbork Synthesis Radio Telescope array we have set a new limit on the flux of neutrinos, summed over all flavors, with energies in excess of 4×10^{22} eV.

I. INTRODUCTION

At high energies the spectrum of cosmic rays follows a power law distribution extending up to extremely large energies. At the Pierre Auger Observatory cosmic rays have been observed [1] with energies in excess of $\sim 10^{20}$ eV. Above the Greisen-Zatsepin-Kuzmin (GZK) energy of 6×10^{19} eV, cosmic rays can interact with the photons of the cosmic microwave background to produce pions [2, 3] which carry a sizable fraction of the original energy of the cosmic ray. Charged pions decay and produce neutrinos and one thus may expect the presence of neutrinos with energies in excess of the GZK energy. Recently at the Pierre Auger Observatory a steepening of the slope in the cosmic ray spectrum has been observed at the GZK energy [1] which can be regarded as a consequence of the GZK effect.

Since neutrinos are chargeless they will propagate in a straight line with negligible energy loss from the location where they have been created to the observer, thus carrying direct information on their source. These sources could be the aforementioned processes related to the GZK effect or, more exotically, decaying supermassive dark-matter particles or topological defects. This last class of models is referred to as top-down (see Stanev [4] for a review).

Because of their small interaction cross section, the detection of cosmic neutrinos calls for extremely large detectors. At GeV energies their cross section is so minute that at a flux given by the Waxman-Bahcall estimate [5] of a few tens of neutrinos per km^2 per year one needs to employ km^3-scale detectors [6, 7]. At higher neutrino energies the reaction cross section increases. However, their flux is expected to fall even faster and one needs even larger detection volumes. These can be obtained by observing large detector masses from a distance. The ANITA balloon mission [8] monitors an area of a million km^2 of South Pole ice and the FORTE satellite [9] can pick up radio signals coming from the Greenland ice mass. Alternatively the Pierre Auger Observatory can distinguish cosmic ray induced air showers from neutrino induced cascades at very high zenith angles [10].

The Moon offers an even larger natural detector volume. In the interaction of an UHE neutrino about 20% of the energy of the neutrino is converted into a cascade of high-energy particles, called the hadronic shower. Due to the electromagnetic component of this shower the electrons in the material are swept out from the atom to become part of the shower. The shower thus has an excess of negative charge moving with relativistic velocities through a material with an index of refraction considerably different from unity resulting in the emission of Cherenkov radiation. Since the lateral side of the shower has a dimension of the order of 10 cm, the radio emission is coherent for wavelength of this magnitude and larger or for frequencies up to ~ 3 GHz. The emission of coherent Cherenkov radiation in such a process is known as the Askaryan effect [11]. This emission mechanism has been experimentally verified at accelerators [12] and extensive calculations have been performed to quantify the effect [13, 14].

For showers in the lunar regolith, the top layer of the Moon consisting of dust and small rocks, its properties are important. Much is known from samples brought from the Moon [15]. The average index of refraction is $n = 1.8$ and the attenuation length is $\lambda_r = (9/\nu[\mathrm{GHz}])$ m for radio waves. The thickness of the regolith is known to vary over the lunar surface. At some depth there is a (probably smooth) transition to solid rock, for which the density is about twice that of the regolith.

At the highest energies the emitted pulse from the

Moon can be observed at Earth with radio telescopes [16]. The first experiments in this direction were carried out with the Parkes telescope [17], later followed by others [18, 19]. A recent project is LUNASKA [20] that is currently performing lunar Cherenkov measurements with the Australia Telescope Compact Array with a 600 MHz bandwidth at 1.2-1.8 GHz. These observations are all performed at relatively high frequencies (2 GHz) where the emission is strongest. At lower frequencies [21] the angular spread of the emission around the Cherenkov angle increases due to finite source effects [22]. When the wavelength is similar to the longitudinal extent of the shower in the lunar rock, a few meters, the angular spread is close to isotropic and the probability of detecting the radio pulse is largest [22]. In our observations we exploit this optimal frequency range around 150 MHz using the Westerbork Synthesis Radio Telescope (WSRT).

II. OBSERVATIONS WITH THE WSRT

The WSRT consists of an array of 14 parabolic antennas of 25 m diameter on a 2.7 km east-west line. In the observations we use the Low Frequency Front Ends (LFFEs) which cover the frequency range 115–180 MHz with full polarization sensitivity. The Pulsar Machine II (PuMa II) backend [23] can record a maximum bandwidth of 160 MHz, sampled as 8 subbands of 20 MHz each. Only 11 of the 12 equally spaced WSRT dishes are used for this experiment which means that when the telescopes are added in phase the resultant beam on the sky is a fan beam[24]. The phases required to add the dishes coherently are determined by observations of a known calibrator source, which at these frequencies is Cassiopeia A. Adjusting the phase relations between the 8 subbands they can be pointed to any location within the primary beam of the 25 m dish. We therefore choose to use 4 frequency bands centered at frequencies of 123, 137, 151 and 165 MHz repeated for two different look directions or beams, aimed at different sides of the Moon, each covering about one third of the lunar surface. This increases the effective aperture and creates the possibility of an anti-coincidence trigger since a lunar Cherenkov pulse should only be visible in one of the two beams. Because of overlap in the band width of the sub-bands the total bandwidth per beam is 65 MHz. The system has a real time automatic gain control (AGC) system, that stabilizes the average gain of the output signal. The time series data is recorded for each subband with a sampling frequency of 40 MHz. The timeseries nature of the data and the lack of calibrated amplitude calibrator signal means that an accurate absolute calibration of the signal strength is not possible and we therefore express the pulse strength in terms of the power of the background noise σ^2, the System Equivalent Flux Density. Averaged over the frequency range under consideration this amounts to $\sigma^2 = 400$ Jy where care has been taken not to have the galactic plane in the field of view.

The data is processed in blocks of 0.1 s, where each block is divided in 200 traces of 20,000 time samples. The data analysis is performed in three steps.

First, the narrow band Radio Frequency Interference (RFI) is filtered from the data. The Fourier transforms of the 200 time traces in one block are added to suppress statistical fluctuations and fitted by a 9^{th} order polynomial. All frequency channels exceeding the fit by 50% or more are marked as RFI lines and set equal to zero. This is done for all 8 frequency bands and both polarizations. The loss of band width due to this filtering is less than 2%.

Second, the dispersion due to the ionosphere of the Earth is corrected for. The vertical total electron content (TEC) values of the ionosphere are provided by the DLR Institut für Kommunikation und Navigation. These values are corrected for the elevation of the Moon to obtain the slanted-TEC (STEC) value. Because of variations of the ionosphere on short timescales and uncertainties in the vertical density profile we allow for an inaccuracy in the determined STEC value. From the STEC value a frequency dependent phase is calculated which is used in the inverse fourier transform to obtain dispersion and RFI corrected time traces. The error in the STEC value may result in an increased time width of the pulses and an offset between the arrival times of pulses in different frequency bands.

Third, the spectrum is searched for strong pulses with large bandwidth. From the corrected time spectra a 5-time-sample-summed relative-power spectrum is constructed,

$$P_5 = \frac{\sum\limits_{5\text{ samples}} P_x}{\left\langle \sum\limits_{5\text{ samples}} P_x \right\rangle} + \frac{\sum\limits_{5\text{ samples}} P_y}{\left\langle \sum\limits_{5\text{ samples}} P_y \right\rangle}, \tag{1}$$

where the averaging is done over one time trace (20,000 time samples), and x and y denote the two polarizations. By summing over 5 time samples one allows for an error in the STEC value and for the spreading of a bandwidth-limited Nyquist-sampled pulse. The P_5-spectra are searched for values exceeding 5. The first and last 250 time samples, corresponding to 0.25% of the observation time, are excluded from this search since the RFI noise is not properly eliminated from these parts of the spectrum. A trigger is generated when in all four frequency bands in the same beam a value $P_5 > 5$ is found, within a maximum time offset of $\Delta t = \text{STEC} \times 40 \frac{(100MHz)^2}{\nu_1 \nu_2} \frac{\nu_2^2 - \nu_1^2}{\nu_1 \nu_2}$ ns, to account for a 30% error on the STEC value (in units of $TECU = 10^{16} el/m^2$). No search is done for a second pulse in the same trace. The value S is defined as the sum over the maximum P_5 values in the 4 frequency bands,

$$S = \sum_{4\text{ bands}} P_5 \, . \tag{2}$$

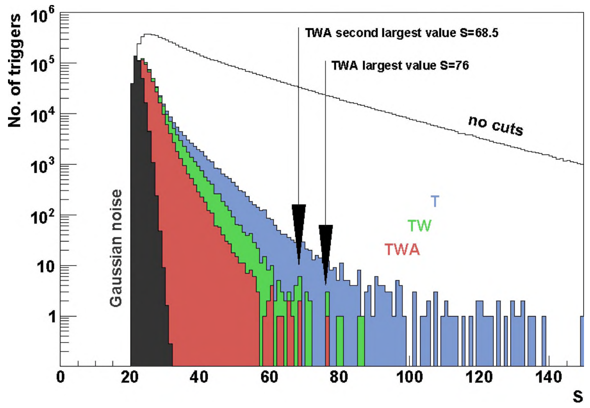

FIG. 1: [color online]Distribution of S for increasingly stronger cuts. The top curve represents the distribution of raw triggers where subsequently the, T, TW, and the TWA cuts are applied.

Fig. 1 shows the distribution of S for the triggered events. In a subsequent analysis additional constraints are imposed.

Timer signal (T) The data contains short strong pulses that repeat at a regular interval with a frequency of 102.4 s^{-1} suggesting an instrumental origin. Cutting out the time intervals in which these pulses occur corresponds to a loss of $\sim$10% of observation time.

P_5 width (W) The number of consecutive P_5 values exceeding the threshold should be limited for a real lunar pulse. On the basis of simulations the width cut is set at $W < 12$.

Anti-coincidence (A) A lunar pulse should be visible in only one of the two beams. An anti-coincidence trigger is set up by excluding events in which a pulse was found in both beams in the same time trace.

Fig. 1 shows distributions of S after application of only the timer cut, the timer and width cut (TW), and a combination of all cuts (TWA). The line enclosing the black area corresponds to the expected number of triggers for pure Gaussian noise. After all cuts have been applied the number of triggers for which $S > 23$ is a factor of 3-4 higher than the amount of triggers expected for Gaussian noise. The largest remaining pulse has a value of $S = 76$ which is used for setting a limit on the flux of UHE neutrinos. This is a factor 3 larger than expected for statistical noise which reflects in less stringent limits that estimated in Ref. [22]. A full account of the analysis will be presented in Ref. [25].

A closer examination of the pulse with $S = 76$ excludes the possibility of it being a lunar pulse. More than half of the total power is received in one of the four frequency bands, while the other bands triggered on pulses that are of comparable size as background pulses. Moreover, the same large peak is present in the corresponding frequency band of the other beam. The anti-coincidence cut did not remove this event since in that beam not all other bands had a trigger, indicating that our limit is rather conservative.

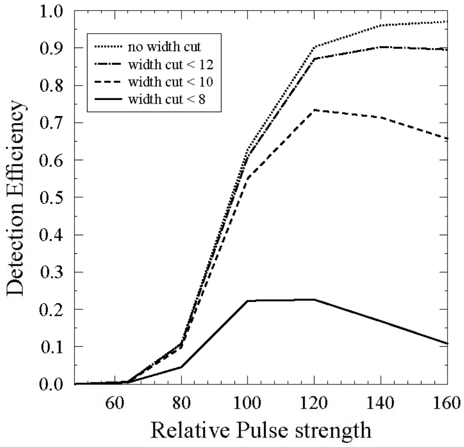

FIG. 2: The detection efficiency is shown as a function of pulse strength for various settings of the trigger conditions as discussed in the text. The dotted curve indicates the efficiency when no width cut is applied.

III. DETECTION EFFICIENCY

To determine our detection efficiency, pulses with a time-duration less than the sampling time are dispersed corresponding to a typical TEC value, simTEC=12. The amplitudes are Nyquist-sampled with a random time offset, rounded off to the nearest integer within the dynamic range, and added to the raw data (considered as background). The detection efficiency (DE) is the fraction of inserted pulses that is retrieved after applying the trigger conditions and the cuts that are used in the analysis. For the simulations we have inserted 1000 pulses in various 10 second segments of data.

Fig. 2 shows the DE for inserted pulses of strength varying from $S_i = 50$ to $S_i = 160$. The pulse from the Moon is polarized in the direction of the shower. In the simulations we have therefore taken into account the Faraday rotation of the polarization vector. The de-dispersion is done with STEC=10, different from simTEC, to simulate an error in the STEC value. The lines in Fig. 2 show the DE for recovering pulses with strength exceeding $S_{th} = 77$. Due to interference from the background the recovered pulse strength differs from the input value S_i. The dotted lines show the DE without any width cut applied. Dash-dotted (dashed, solid) lines represents the DE with width cut $W < 12$, ($W < 10$, $W < 8$) respectively. Clearly the $W < 12$ is close to the optimum and is selected for further analysis.

After correcting for hardware and software failures, excluding four observation runs which have exceptionally large numbers of raw triggers, correcting for dead time due to double hits, and the effect of timer signal correction, we have 46.7 hours of dual-beam observation time left. Each beam covers about a third of the lunar area.

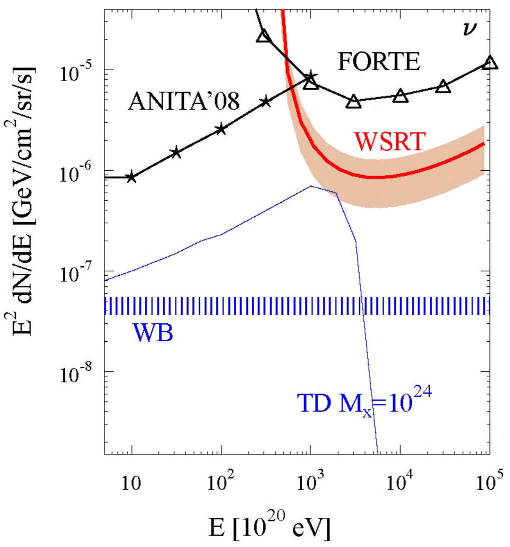

FIG. 3: [color online] The currently established neutrino flux limit is compared to the limits set by ANITA [8] and FORTE [9] as well as the Waxman-Bahcall flux [5] and a TD model prediction [26]. The band shows the systematic error.

IV. RESULTS

In 46.7 hours of observation time no pulses from the Moon were found for which $S > 77$. To convert this into a probability for not observing a pulse from the Moon we use Fig. 2 which shows that only pulses with strength in excess of $S_i > 120$ have a large DE of 87.5%. For smaller pulses from the Moon, due to interference with background, the DE drops rapidly which will give rise to less constraining limits.

With the applied constraints we thus have a 87.5% probability to observe an emitted pulse with $S_i > 120$ corresponding to $120\sigma^2 \times 5 = 240$ kJy. The lack of pulses of a certain power implies a limit on the flux of neutrinos. This is not a simple algebraic relation since attenuation of the signal in the Moon, transmission at the lunar surface and angle with respect to the direction of the neutrino all affect the observed pulse strength. On the basis of the simulations which are described in detail in Ref. [22] the 90% confidence limit flux limit shown in Fig. 3 has determined. In arriving at this the model-independent procedure described in Ref. [9] has been followed.

In arriving at this limit the same assumptions have been made as in Ref. [22], in particular that the neutrino cross sections equal the predictions given in Ref. [27]. The estimated systematic errors on the acceptance simulation [22] are due to uncertainties in the: density (10% in threshold energy), attenuation length (40% in flux), and stopping power of the regolith, (20% in flux). The error in the moon coverage of the two beams is estimated at 20%. Adding these errors in quadrature gives a systematic error on the flux of 50% as indicated in Fig. 3.

The present limits in the UHE region have been set by ANITA [8] and FORTE [9]. On the basis of the present observations the flux limits have been improved by an order of magnitude at the highest energies. The new limit is still well above the Waxman-Bahcall limit [5] but borders on the predictions of a top-down model [26] for exotic particles of mass $M_X = 10^{24}$ eV.

Presently similar techniques as used in the WSRT observations are implemented for observations with the LOFAR radio telescope (presently being rolled out) and the future SKA telescope. With the latter we should be able to observe neutrinos associated with the GZK effect [28].

Acknowledgments

This work was performed as part of the research programs of the Stichting voor Fundamenteel Onderzoek der Materie (FOM) and of ASTRON, both with financial support from the Nederlandse Organisatie voor Wetenschappelijk Onderzoek (NWO).

---

[1] J. Abraham et al., Phys. Rev. Lett. **101**, 061101 (2008).
[2] K. Greisen, Phys. Rev. Lett. **16**, 748 (1966).
[3] G. Zatsepin and V. Kuzmin, Pis'ma Zh. Eksp. Teor. Fiz. **4**, 114 (1966).
[4] T. Stanev, astro-ph/0411113 (2004).
[5] E. Waxman and J. N. Bahcall, Phys. Rev. **D59**, 023002 (1999), hep-ph/9807282.
[6] J. Ahrens et al., Nucl. Phys. Proc. Suppl. **118**, 388 (2003).
[7] U. Katz et al., Nucl. Instrum. Meth. **A567**, 457 (2006).
[8] P. Gorham et al. (ANITA), Phys. Rev. Lett. **103**, 051103 (2009).
[9] H. Lethinen et al., Phys. Rev. D **69**, 013008 (2004).
[10] J. Abraham et al. (The Pierre Auger), Phys. Rev. Lett. **100**, 211101 (2008), 0712.1909.
[11] G. Askaryan, Sov. Phys., J.E.T.P. **14**, 441 (1962).
[12] D. Saltzberg et al., Phys. Rev. Lett. **86**, 2802 (2001).
[13] E. Zas, F. Halzen, and T. Stanev, Phys. Rev. D **45**, 362 (1992).
[14] J. Alvarez-Muñiz and E. Zas, Phys. Lett. B **411**, 218 (1997).
[15] G. Olhoeft and D. Strangway, Earth Plan. Sci. Lett. **24**, 394 (1975).
[16] R. Dagesamanskii and I. Zheleznyk, Sov. Phys. J.E.T.P. **50**, 233 (1989).
[17] T. Hankins, R. Ekers, and J. O'Sullivan, MNRAS **283**, 1027 (1996).
[18] P. Gorham et al., Phys. Rev. Lett. **93**, 41101 (2004).
[19] A. Beresnyak et al., Astronomy Reports **49**, 127 (2005).
[20] C. W. James et al. (2009), 0906.3766.
[21] H. Falcke and P. Gorham, Astropart. Phys. **19**, 477 (2003).

[22] O. Scholten et al., Astropart. Phys. **26**, 219 (2006).
[23] R. Karuppusamy, B. Stappers, and W. van Straten (2008), 0802.2245.
[24] G. H. Janssen et al. (2009), 0902.1675.
[25] S. Buitink et al., in preparation (2009).
[26] R. Protheroe and T. Stanev, Phys. Rev. Lett. **77**, 3708 (1996).
[27] R. Gandhi, Nucl. Phys. **B91**, 453 (2000).
[28] O. Scholten et al., Nucl. Inst. and Meth. **A604**, s102 (2009).